doi.org/10.36721/PJPS.2026.39.12.354.1

Polydopamine nanoparticles carrying bergenin inhibit the malignant biological behavior of glioma through inhibiting the CASC11/AKT3 axis

Kaihua Yang and Leyuan Zhou*
Department of Radiation Oncology, Affiliated Hospital of Jiangnan University, Wuxi, Jiangsu, 214000, China

Abstract: **Background**: Bergenin (BN), a C-glucoside of 4-O-methyl gallic acid, exhibits a broad spectrum of pharmacological activities, including notable antioxidant, anti-inflammatory and anticancer effects. **Objectives**: This study aimed to explore the impact of polydopamine nanoparticles loaded with bergenin (PDANPs-BN) on glioma and their mechanisms of action. **Methods**: PDANPs-BN nanocomposites were prepared and U251 cells were cultured and divided into the BN group and the PDANPs-BN group. The biological processes of U251 cells were observed by using CASC11 mimic, si-CASC11 and agonists and inhibitors of AKT3. **Results**: Compared to free BN, PDANPs-BN significantly inhibited the malignant biological behavior of U251 cells, reducing the cell proliferation rate by approximately 45% and suppressing migration capacity by about 60% (P<0.05). Mechanistic studies revealed that PDANPs-BN downregulated CASC11 expression levels by 2.1-fold, thereby inhibiting AKT3 signaling pathway activity. The strongest antitumor effect was observed when combined with si-CASC11 and an AKT3 inhibitor. While the addition of an AKT3 agonist partially reversed this effect, cell proliferation remained suppressedand colony-forming ability was altered. **Conclusion**: PDANPs-BN acts by targeting the CASC11/AKT3 axis, resulting in downregulation of CASC11 and consequent inhibition of AKT3 signaling, which ultimately curbs the malignant progression of glioma.

Keywords: Bergenin; CASC11/AKT3; Glioma; Petrosin; Polydopamine nanoparticles

Submitted on 27-06-2024 – Revised on 21-01-2026 – Accepted on 13-02-2026 – Available online on 01-09-2026 – Published on 01-12-2026

INTRODUCTION

Glioma, the most prevalent and aggressive primary malignant tumor of the central nervous system, originates from glial cells and is characterized by rapid infiltration, high recurrence rates and a dismal prognosis despite multimodal therapeutic regimens including surgery, radiotherapy and chemotherapy (Read *et al*., 2024). This persistent clinical challenge underscores an urgent need to elucidate the precise molecular drivers of glioma progression and to develop novel targeted therapeutic strategies.

In recent years, long non-coding RNAs (lncRNAs) have emerged as pivotal regulators in tumorigenesis and potential therapeutic targets. Among them, cancer susceptibility candidate 11 (CASC11) has been identified as a potent oncogenic lncRNA in various cancers, including colorectal and hepatocellular carcinoma, where it promotes tumor growth and metastasis primarily by activating key signaling pathways such as Wnt/β-catenin and PI3K/AKT (Wang *et al*., 2020; Zheng *et al*., 2021). Notably, in glioma, elevated CASC11 expression has been linked to enhanced cell proliferation, migration and survival. Mechanistically, CASC11 interacts with PDK1, leading to the phosphorylation and activation of AKT3—a brain-enriched serine/threonine kinase that plays a central role in the oncogenic PI3K/AKT/mTOR signaling cascade (Zhuo *et al*., 2025). Thus, the CASC11/AKT3 axis represents a promising yet underexploited therapeutic target for intervening in glioma malignancy.

Concurrently, natural compounds with multi-target potential have garnered significant attention for cancer therapy. Bergenin (BN), a C-glucoside of 4-O-methyl gallic acid, exhibits a broad spectrum of pharmacological activities, including notable antioxidant, anti-inflammatory and anticancer effects (Li *et al*., 2023). Preclinical studies across various cancer models have demonstrated that BN can suppress tumor growth by modulating key signaling pathways, including PPARγ/PTEN/Akt and Wnt/β-catenin (Cao *et al*., 2024; He *et al*., 2023). These properties position BN as a promising candidate for glioma treatment. However, its clinical translation is severely hampered by inherent physicochemical limitations, including poor aqueous solubility, instability under physiological conditions, susceptibility to rapid degradation and consequently, low bioavailability and insufficient tumor accumulation (Li *et al*., 2025).

Nanotechnology offers a viable strategy to overcome these delivery challenges. Polydopamine nanoparticles (PDA NPs) have emerged as a versatile and attractive drug delivery platform due to their excellent biocompatibility, ease of surface functionalization, strong adhesive properties and ability to protect encapsulated therapeutic agents from degradation (Bashir *et al*., 2022; Lin *et al*.,

**Corresponding author:* e-mail: mufei0246385508@126.com

2022). Loading BN onto PDA NPs (forming PDANPs-BN) is therefore anticipated to enhance drug stability, prolong systemic circulation, improve passive tumor targeting via the enhanced permeability and retention (EPR) effect and ultimately potentiate the intracellular delivery and therapeutic efficacy of BN (Mahata *et al*., 2025).

Despite these individual advances, critical knowledge gaps remain at their intersection. While BN shows antitumor potential and the CASC11/AKT3 axis is implicated in glioma progression, it remains unknown whether BN acts in glioma by specifically targeting this oncogenic axis. Furthermore, although nano-formulation can enhance drug delivery, it remains unexplored whether a PDANPs-BN system can specifically and effectively downregulate the expression of oncogenic lncRNA CASC11 and inhibit its downstream effector AKT3 in glioma cells, thereby achieving superior antitumor outcomes compared to free BN.

Based on this rationale, it was hypothesized that the CASC11/AKT3 signaling axis is a key driver of glioma malignancy and can be effectively targeted by BN. This study further proposed that nano-encapsulating BN within PDANPs will not only overcome the delivery limitations of free BN but also enhance its therapeutic efficacy by specifically facilitating the downregulation of CASC11 and the subsequent inhibition of AKT3 activation. This study aimed to validate this hypothesis by evaluating the effects of PDANPs-BN on glioma cell behavior and elucidating the underlying mechanisms involving the CASC11/AKT3 axis.

MATERIALS AND METHODS

Instruments and reagents

The following cell lines, reagents and instruments were used in this study. A full list of abbreviations is provided in table 1. Human glioma U251 cells were obtained from Shenzhen Haodi Huatuo Biotech (Shenzhen, China). Bergenin (BN) was purchased from Shanghai Yuanye Biotech (Shanghai, China). The CASC11 mimic, si-CASC11, negative controls and the MTT kit were sourced from Shanghai Yaji Biotech (Shanghai, China). The AKT3 agonist (SC79) and AKT3 inhibitor (GSK690693) were procured from Selleck Chemicals (Houston, TX, USA). Dopamine hydrochloride was obtained from Sigma-Aldrich (Shanghai, China) and Lipofectamine™ 3000 transfection reagent was acquired from Invitrogen (Carlsbad, CA, USA). Cell culture dishes were purchased from Zhejiang Zhongzai Medical (Zhejiang, China) and the CCK-8 kit was procured from Yeiyi Saint Biotechnology (Shanghai, China). Transwell chambers were obtained from Beijing Daco Biotech (Beijing, China). RIPA lysis buffer and the BCA protein concentration assay kit were sourced from Beyotime Biotechnology (Shanghai, China), while primary and secondary antibodies were obtained from Zhongshan Golden Bridge Biotechnology (Beijing, China).

The following instruments were used for characterization and analysis: a flow cytometer [Model: CytoFLEX, Beckman Coulter, USA] was sourced from Shanghai Yuanyao Biotechnology (Shanghai, China); an inverted microscope [Model: CKX53, Olympus, Japan] was provided by Shanghai Fulai Optical Technology (Shanghai, China); a transmission electron microscope [Model: HT7800, Hitachi, Japan] was procured from Wuxi Bohe Biotech (Wuxi, China); a scanning electron microscope [Model: Regulus 8100, Hitachi, Japan] was also utilized. A dynamic light scattering (DLS) system [Model: Zetasizer Nano ZS, Malvern Panalytical, UK] was employed for particle size and zeta potential measurements. Fourier transform infrared spectroscopy [Model: Nicolet iS50, Thermo Fisher Scientific, USA] was performed for chemical characterization. Ultraviolet-visible spectrophotometry [Model: UV-2600i, Shimadzu, Japan] was used to determine drug loading and encapsulation efficiency. PCR amplification was conducted using a real-time PCR system [Model: Quant Studio 3, Applied Biosystems, USA] and chemiluminescence imaging for Western blotting was performed using a gel documentation system [Model: ChemiDoc XRS+, Bio-Rad, USA]. PCR primers and the kit were provided by Shanghai Fusheng Industrial (Shanghai, China) and the RNA extraction kit was purchased from Beijing Kangrun Chengye Biotechnology (Beijing, China).

Preparation of nanomaterials

A nanoparticle carrier preparation method based on dopamine self-polymerization was referenced and modified (Hu *et al*., 2024). Specifically, 200 mg of BN was precisely weighed, added to 10 mL of distilled water and stirred until completely dissolved to obtain a homogeneous BN solution with a concentration of 20 mg/mL. The PDA solution was then placed in an ultrasonic cleaner to remove insoluble impurities and bubbles, forming a uniform PDA precursor solution. The cleaned solution was transferred to a water bath maintained at 70-80°C and continuously stirred to further diffuse the PDA molecular chains and form nanoparticles. The BN solution was slowly added to the total PDA solution and thoroughly stirred until completely mixed. Ultracentrifugation was performed to remove unreacted substances. Finally, the nanoparticle sample was dried to obtain the composite sample of PDANPs-BN (the preparation process is shown in Fig. 1). The hydration particle size, zeta potential and polydispersity index (PDI) of PDANPs-BN were measured using dynamic light scattering (DLS). The morphology of the nanoparticles was observed by transmission electron microscopy (TEM) and scanning electron microscopy (SEM). Successful compounding of BN with PDA NPs was analyzed using Fourier transform infrared spectroscopy (FTIR). The drug loading (DL) and

encapsulation efficiency (EE) of the nanoparticles were calculated by ultraviolet spectrophotometry. Specifically, the absorbance of the samples was measured at a wavelength of 267 nm using a UV-Vis spectrophotometer [Model: UV-2600i, Shimadzu, Japan]. The concentration of BN was determined from a standard calibration curve prepared with known concentrations of free BN in the same solvent system.

Cell culture and grouping

The human glioma U251 cell line was resuscitated and maintained in high-glucose DMEM supplemented with 10% fetal bovine serum and 1% penicillin-streptomycin solution. Cells were cultured as an adherent monolayer in a humidified incubator at 37°C with 5% CO_2. Experiments were conducted using cells in the logarithmic growth phase (approximately 80–90% confluent) with optimal growth conditions. The experimental groups were designed as follows: Blank group: cells were treated with fresh complete medium containing no drugs or nanomaterials. BN group: cells were treated with fresh complete medium containing BN solution at a final concentration of 20 μg/mL and co-incubated for 24 hours. PDANPs-BN group: cells were treated with fresh complete medium containing the PDANPs-BN nanoparticle suspension, with a final BN concentration matching that of the BN group (20 μg/mL) and co-incubated for the same duration (24 hours).

Transfection: According to the Lipofectamine™ 3000 kit instructions, the CASC11 overexpression plasmid CASC11 mimics was transfected into U251 cells. After 6 hours, the cells were continuously cultured in DMEM medium for 48 hours. The knockdown or overexpression efficiency of CASC11 was validated by qRT-PCR. Subsequent experiments were conducted only when the transfection efficiency exceeded 70%.

Cell growth rate detection

Cell growth rate was measured using the MTT assay, as previously described with minor modifications (Moradi *et al*., 2024). U251 cells in the logarithmic growth phase were harvested and seeded into 96-well plates at a density of 5×10^4 cells/well (100 μL). After complete cell adhesion, the original medium was removed and replaced with fresh medium containing the corresponding drug treatments according to the experimental groups. Each treatment group contained at least five replicate wells. Following incubation for 24, 48 and 72 hours, 20 μL of MTT solution was added to each well and the plates were further incubated for 4 hours. The supernatant was carefully aspirated and 150 μL of DMSO was added to each well. The plates were then placed on a shaker and gently agitated for 10 minutes to fully dissolve the formazan crystals. The absorbance of each well was measured at 570 nm using a microplate reader. The cell growth rate was calculated as (Absorbance of treatment group - Absorbance of blank control group) / Absorbance of control group × 100%.

Proliferation ability detection

Cell proliferation capacity was assessed using the Cell Counting Kit-8 (CCK-8) according to the manufacturer's instructions and established protocols (Han *et al.,* 2024). U251 cells in the logarithmic growth phase were inoculated into a 96-well plate at a density of 1×10^3 cells/well (200 μL). After cell adhesion, drug treatments were administered in accordance with the experimental design. Then, 10 μL of CCK-8 reagent was added to each well and the plate was returned to the incubator for protected light incubation for 4 hours. When the solution color turned orange-red, the absorbance at 450 nm was measured using a microplate reader. The optical density (OD) value at 450 nm was considered directly proportional to the number of viable cells.

Testing of plate colony formation ability

The plate colony formation assay was performed following the standard method described by Brix *et al*. (2021) and as applied in recent studies (Yan *et al*., 2020). U251 cells in the logarithmic growth phase were harvested and seeded into 6-well plates at a density of 1×10^3 cells/well (2 mL). The cells were then incubated undisturbed, with the culture medium replaced with fresh medium every 3 days. After 14 days of continuous culture, the medium was discarded and the cells were gently rinsed twice with 1X PBS. Each well was fixed with 1 mL of 4% paraformaldehyde at room temperature for 15 minutes. After removing the fixative, the cells were stained with 1 mL of 0.1% crystal violet solution for 30 minutes at room temperature. The staining solution was then discarded and the plates were gently rinsed under running water until the background became colorless. The plates were air-dried inverted at room temperature, photographed and statistically analyzed using ImageJ software.

Migration and invasion ability detection

Migration and invasion assays were conducted using the Transwell system (Zhao *et al*., 2022).

Migration assay: U251 cells in the logarithmic growth phase were seeded into the upper chamber of a Transwell system at a density of 5×10^4 cells/well. The lower chamber was filled with 600 μL of complete medium containing 10% FBS as a chemoattractant. The plates were incubated at 37°C for 24 hours. After incubation, the chambers were carefully removed and non-migrated cells on the inner surface of the membrane were gently wiped away with a cotton swab. The chambers were fixed with 4% paraformaldehyde for 15 minutes and then stained with 0.1% crystal violet for 20 minutes. After rinsing with PBS, cells that had migrated through the membrane were imaged and counted under an inverted microscope in five randomly selected fields of view.

Table 1: Abbreviations list.

Full name	Abbreviation
Bergenin	BN
Polydopamine nanoparticles	PDA NPs
Polydopamine nanoparticles carrying bergenin	PDANPs-BN
Cancer susceptibility candidate 11	CASC11
AKT serine/threonine kinase 3	AKT3
small interfering RNA targeting CASC11	si-CASC11
Human glioma cell line U251	U251
Quantitative real-time polymerase chain reaction	qRT-PCR
Western blot	WB
Propidium iodide	PI
Fluorescein isothiocyanate	FITC
Glyceraldehyde-3-phosphate dehydrogenase	GAPDH
Dulbecco's modified eagle medium	DMEM
Stromal cell-derived factor-1α	SDF-1α
Phosphate buffered saline	PBS
Bicinchoninic acid assay	BCA

Table 2: Real-time PCR primers and primer sequences.

Primer		Sequences
CASC11	Forward primer	5'-AGCTGGGAGTGAAATGTGC-3'
	Reverse primer	5'-GTGATGTTTGGCGGACTCTG-3'
AKT3	Forward primer	5'-ATGAGCGACGTGGCTATTGG-3'
	Reverse primer	5'-TTACCCACAGCATGTCCACTT-3'
GAPDH	Forward primer	5'-TTGCCATTGCACAACTCTTTT-3'
	Reverse primer	5'-AGTGATGGCATGGACTGTGG-3'

Invasion assay: The experimental procedure for the invasion assay was largely identical to the migration assay, with the following critical modification: prior to cell seeding, the polycarbonate membrane of the Transwell upper chamber was uniformly coated with 50–100 μL of diluted Matrigel matrix gel and allowed to solidify at 37ºC for 4–6 hours to simulate an extracellular matrix barrier.

Detection of apoptotic changes by flow cytometry

Cell apoptosis was quantitatively analyzed using the Annexin V-FITC/PI double staining kit following the manufacturer's protocol and established methodology (Zheng *et al*., 2025). Cells from each experimental group were collected, washed twice with pre-cooled PBS and resuspended in 1X Binding Buffer to adjust the cell concentration to 1×10^6/mL. Then, 100 μL of the cell suspension was transferred to a flow cytometry tube, followed by the sequential addition of 5 μL Annexin V-FITC and 5 μL PI staining solution. After gentle mixing, the samples were incubated at room temperature for 15 minutes in the dark. Subsequently, 400 μL of 1X Binding Buffer was added to each tube and the samples were immediately analyzed within 1 hour using a flow cytometer. Data were processed with FlowJo software, where the Annexin V^+/PI^- quadrant represented early apoptotic cells and the Annexin V^+/PI^+ quadrant indicated late apoptotic and necrotic cells.

qRT-PCR detection

Total RNA was extracted using the TRIzol method and reverse transcription was performed using the PrimeScript RT kit (Petrillo *et al*., 2020). The reaction conditions were as follows: 15 minutes at 37ºC and 5 seconds at 85ºC. The PCR reaction mixture contained SYBR Premix ExTaq 10 μL, upstream and downstream primers 0.8 μL each, cDNA template 2 μL and RNase-free water 6.4 μL. pre-denaturation was performed at 95ºC for 30 seconds, followed by 40 cycles of PCR (95ºC for 5 seconds, 60ºC for 30 seconds) and a dissociation curve stage. GAPDH was used as the internal reference gene and the relative expression level of the target gene was calculated by the $2^{-\Delta\Delta Ct}$ method. All experiments were set with three technical replicates. Table 2 lists the primers and primer sequences.

CRISPR-Cas9 technology gene knockout

According to literature reports and operating guidelines (Hu *et al*., 2022), CRISPR/Cas9 gRNA technology mainly included the following steps: design and selection of gRNA library, PCR amplification of gRNA library, lentiviral packaging and infection of gRNA library, identification and screening of gRNA library, PCR exponential amplification and NGS sequencing and analysis. The details were as follows: The gene editing technology CRISPR/Cas9 system was used to design and construct

sgRNA targeting the second exon of the target gene CASC11 and T7 RNA polymerase was used to transcribe Cas9 mRNA *in-vitro*. After the cell line was transfected with sgRNA and Cas9 mRNA *in-vitro*, the target gene was knocked out. Seventy-two hours after transfection, the efficiency of gene editing was verified using the T7EI endonuclease assay and sequencing.

Western blot detection

Total protein was extracted from cells using RIPA lysis buffer supplemented with protease and phosphatase inhibitors. Protein concentration was determined using the BCA protein assay kit (Smith *et al*., 1985). Equal amounts of protein samples (typically 20-40 µg) were separated by sodium dodecyl sulfate-polyacrylamide gel electrophoresis (SDS-PAGE) and subsequently transferred onto polyvinylidene difluoride (PVDF) membranes (Towbin *et al.,* 1979). The membranes were blocked with 5% non-fat milk in Tris-buffered saline containing 0.1% Tween-20 (TBST) for 2 hours at room temperature to prevent non-specific binding. Subsequently, the membranes were incubated overnight at 4ºC with the following primary antibodies diluted in blocking buffer: anti-CASC11 (1:1000), anti-AKT3 (1:1000) and anti-GAPDH (1:1000) as a loading control. After washing three times with TBST, the membranes were incubated with appropriate horseradish peroxidase (HRP)-conjugated secondary antibodies (1:2000 dilution) for 2 hours at room temperature. Protein bands were visualized using an enhanced chemiluminescence (ECL) detection reagent according to the manufacturer's instructions and images were captured using a chemiluminescence imaging system. The intensity of the protein bands was quantified using ImageJ software (National Institutes of Health, USA) and the relative protein expression levels were normalized to GAPDH.

Statistical analysis

The data obtained in each of the above experiments were analyzed using SPSS 21.0 and GraphPad Prism. Unless otherwise stated, $P < 0.05$ was used as the test standard.

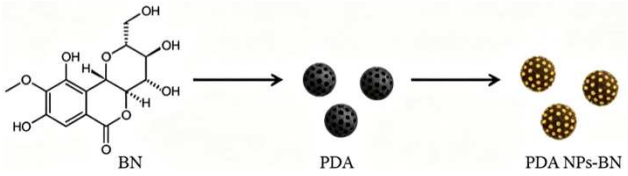

Fig. 1: Preparation of PDANPs-BN nanoparticles.

RESULTS

Nano characterization

The morphology of the nanoparticles was examined by TEM (Fig. 2A) and SEM (Fig. 2B). PDA NPs-BN exhibited a regular spherical or near-spherical structure with uniform distribution and no significant aggregation. DLS results showed that the average hydration particle size of PDA NPs-BN was (173.45 ±3.57) nm (Fig. 2C), the zeta potential was (−28.15±1.01) mV (Fig. 2D) and the PDI was (0.15 ± 0.02), indicating uniform particle size, narrow distribution and good colloidal stability. FTIR analysis (Fig. 2E) revealed that free BN displayed characteristic peaks at 1604 cm^{-1}, 1350 cm^{-1} and 1036 cm^{-1}, corresponding to carbonyl (C=O) and benzene ring (C=C) stretching vibrations. In the FTIR spectrum of PDA NPs-BN, the broad characteristic peaks of PDA NPs were retained, while the main absorption peaks of BN were clearly observed with slight shifts in peak positions. The drug loading performance of PDA NPs-BN was evaluated using ultraviolet spectrophotometry. The results demonstrated an EE of (85.4 ± 2.1)% and a DL capacity of (12.7 ± 0.5)%. These findings indicated that PDA NPs-BN efficiently encapsulates BN and exhibits high drug loading efficiency.

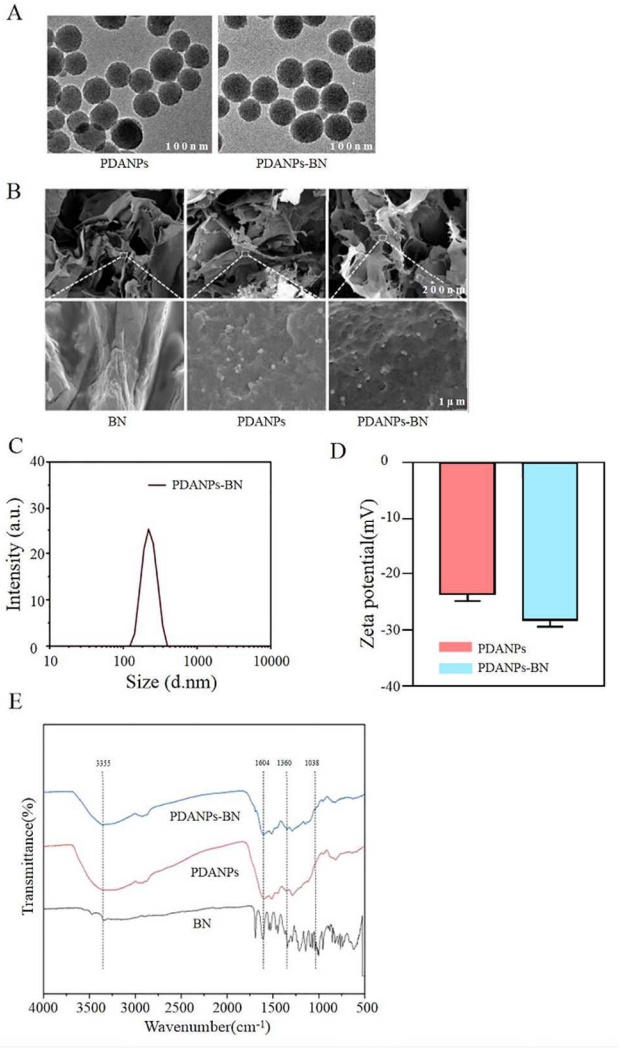

Fig. 2: Characterization of PDANPs-BN nanoparticles. (A) TEM image of PDANPs-BN; scale bar = 100 nm; (B) SEM image of PDANPs-BN; (C) Size distribution of PDANPs-BN; (D) Zeta potential results of PDANPs-BN; (E) FTIR spectrum of PDANPs-BN.

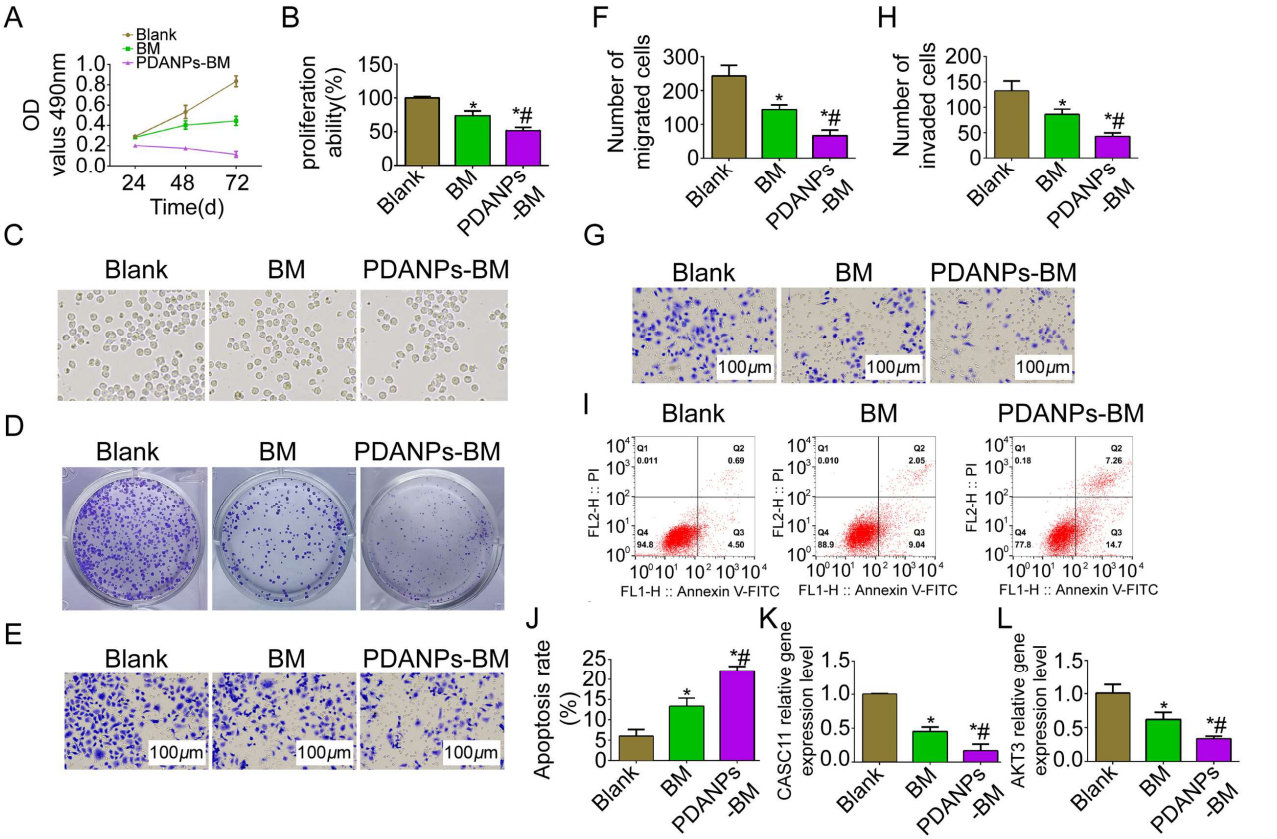

Fig. 3: PDANPs-BN affects the malignant biological behavior of glioma through the CASC11/AKT3 axis. (A) Cell growth rate was detected by MTT assay; (B) Cell proliferation ability was detected by CCK-8 assay; (C) Cell morphology was observed by MTT assay; (D) Colony formation ability was detected by plate colony formation assay; (E and F) Cell migration ability was detected by Transwell assay; (G and H) Cell invasion ability was detected by Transwell assay; (I and J) Cell apoptosis was detected by flow cytometry; (K) Relative gene expression levels of CASC11 and AKT3 were detected by qRT-PCR; (L) Protein expression levels of CASC11 and AKT3 were detected by Western blot. Compared with the blank group, $P < 0.05$; compared with the BN group, #$P < 0.05$; $n = 9$.

PDANPs-BN affects the malignant biological behavior of glioma through the CASC11/AKT3 axis

To explore the impact of BN on glioma, cell intervention experiments were conducted the growth rate of U251 cells was significantly decreased (Fig. 3A). Compared to the blank group, free BN only mildly inhibited cell viability, whereas PDANPs-BN treatment for 24 hours significantly reduced cell proliferation activity by 52.7% ± 4.1% (vs. control group, *$P < 0.05$; vs. BN group, #$P < 0.05$) (Fig. 3B). The subsequent comparison results U251 cells under PDANPs-BN intervention conditions were observed to gradually become round (Fig. 3C) and the plate colony formation ability of U251 was significantly inhibited (Figs. 3C and 3D); further exploration found that the migration and invasion abilities of U251 cells under PDANPs-BN intervention conditions were inhibited (Figs. 3E-3G) and PDANPs-BN significantly inhibited cell migration and invasion by 71.5% ± 6.0% and 68.3% ± 5.2%, respectively (all $P < 0.05$), demonstrating markedly superior efficacy compared to the BN group (Figs. 3F-3H). Moreover, flow cytometry results revealed that PDANPs-BN induced an apoptosis rate of up to 28.4% ± 2.5%, approximately 5.2-fold higher than the control group and 2.1-fold higher than the BN group ($P<0.05$, Figs. 3I and 3J). Western blot analysis revealed that compared with the control group, PDANPs-BN treatment significantly downregulated the protein expression levels of CASC11 and AKT3 by 65% and 50%, respectively ($P < 0.05$) (Figs. 3K and 3L).

CASC11/AKT3 axis is involved in the process of PDANPs-BN inhibiting the malignant biological behavior of glioma

Based on the above findings, the mechanism of PDANPs-BN in the malignant biological behavior of glioma was further explored. After intervention with CASC11mimin, the growth rate of U251 cells was found to be increased (vs. blank group, $P > 0.05$, Fig. 4A), while the proliferation ability was significantly improved (Fig. 4B). The aforementioned indicator levels of U251 cells after si-CASC11 intervention were opposite to those observed with CASC11mimin (Figs. 4A and 4B), accompanied by the gradual rounding of U251 cells (Fig. 4C) and an inhibitory effect on the plate colony formation ability of U251 cells (Fig. 4D).

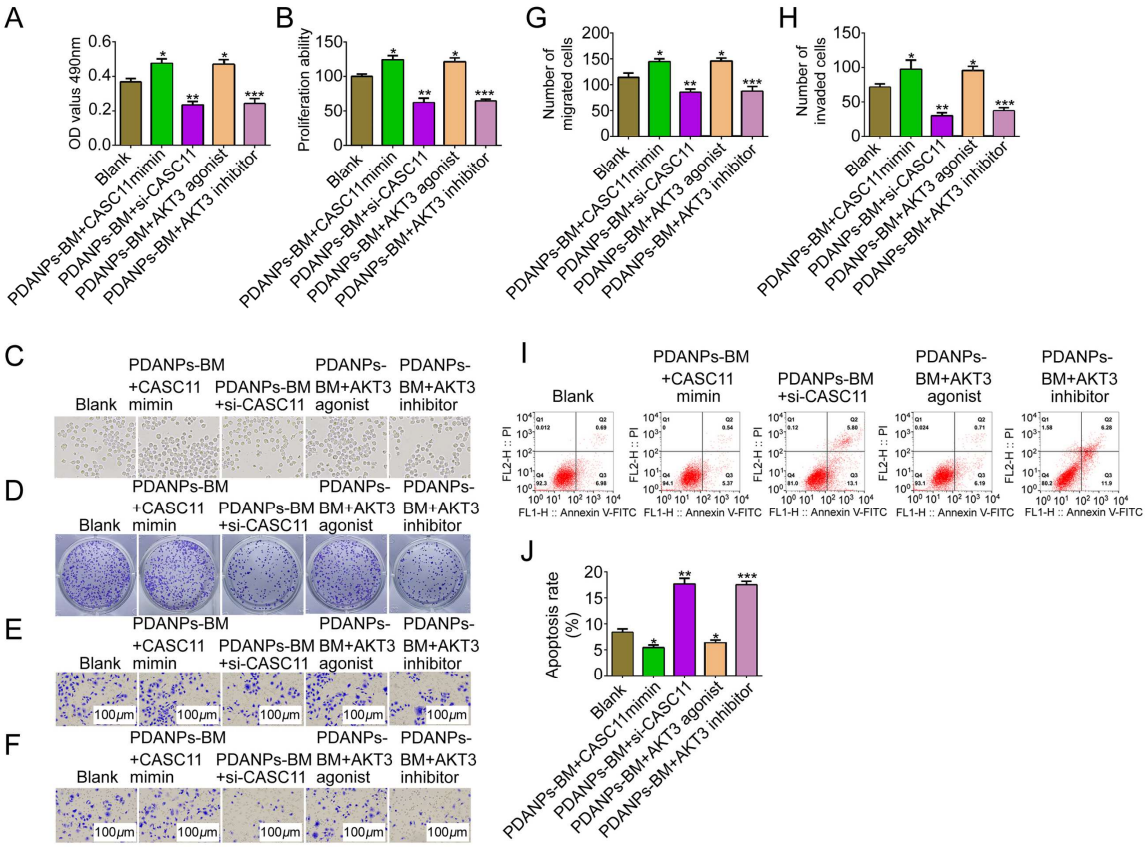

Fig. 4: The CASC11/AKT3 axis is involved in the process of PDANPs-BN inhibiting the malignant biological behavior of glioma. (A) MTT method to detect cell growth rate; (B) CCK-8 to detect cell proliferation ability; (C) MTT method to detect cell morphology; (D) Plate colony formation assay to detect cell formation ability; (E and F) Transwell detects cell migration ability; (G and H) Transwell detects cell invasion ability; (I, J) Flow cytometry detects cell apoptosis; compared with the blank group, *P<0.05; and PDANPs-BN compared with the +CASC11mimin group, **P<0.05; compared with the PDANPs-BN+AKT3 group, ***P<0.05; n=9.

The inhibition of migration and invasion was affected by si-CASC11, resulting in a 65.2% reduction in cell migration capacity (Figs. 4E-4H), while apoptosis was significantly enhanced, with an observed apoptosis rate of 18.5% (Figs. 4I and 4J), indicating that si-CASC11 played a key role under PDANPs-BN intervention conditions. To further explore the role of AKT3 in this process, AKT3 agonists and AKT3 inhibitors were used to intervene in U251 cells under PDANPs-BN intervention conditions. The results showed that the relevant outcomes under AKT3 inhibitor intervention conditions and the change trends were consistent with those observed under si-CASC11 intervention conditions (Figs. 4A-4J). The above experimental results reflect that downregulating the expression of the CASC11/AKT3 axis can, to a certain extent, promote the inhibitory effect of PDANPs-BN on the malignant biological behavior of glioma.

The mechanism of PDANPs-BN slowing down the malignant biological behavior of glioma through the CASC11/AKT3 axis

An AKT3 activator was added to the si-CASC11 + AKT3 inhibitor intervention. The growth rate of U251 cells was found to show a decreasing trend and the cell proliferation ability was also significantly decreased (Figs. 5A and 5B). At the same time, after si-CASC11 + AKT3 inhibition under the intervention conditions of agent + AKT3 activator, the morphology of U251 cells was altered (Fig. 5C) and the plate colony formation ability of the cells was promoted (Fig. 5D). Further observation of the malignant biological behavior of U251 revealed that migration and invasion were both reduced, with the PDANPs-BN + si-CASC11 + AKT3 inhibitor group exhibiting the strongest inhibitory ability (Figs. 5E-5H). At the same time, the apoptosis ability was also significantly reduced and the apoptosis rate was significantly decreased (vs. other groups, $P < 0.05$, Figs. 5I and 5J). Furthermore, the expression of CASC11/AKT3 was significantly reduced (Figs. 5K and 5L) and the protein levels also showed consistent changes (Fig. 5M). This further verified that PDANPs-BN downregulates the expression of CASC11/AKT3 and inhibits the malignant biological behavior of glioma, thereby slowing down disease progression (as summarized in Fig. 5).

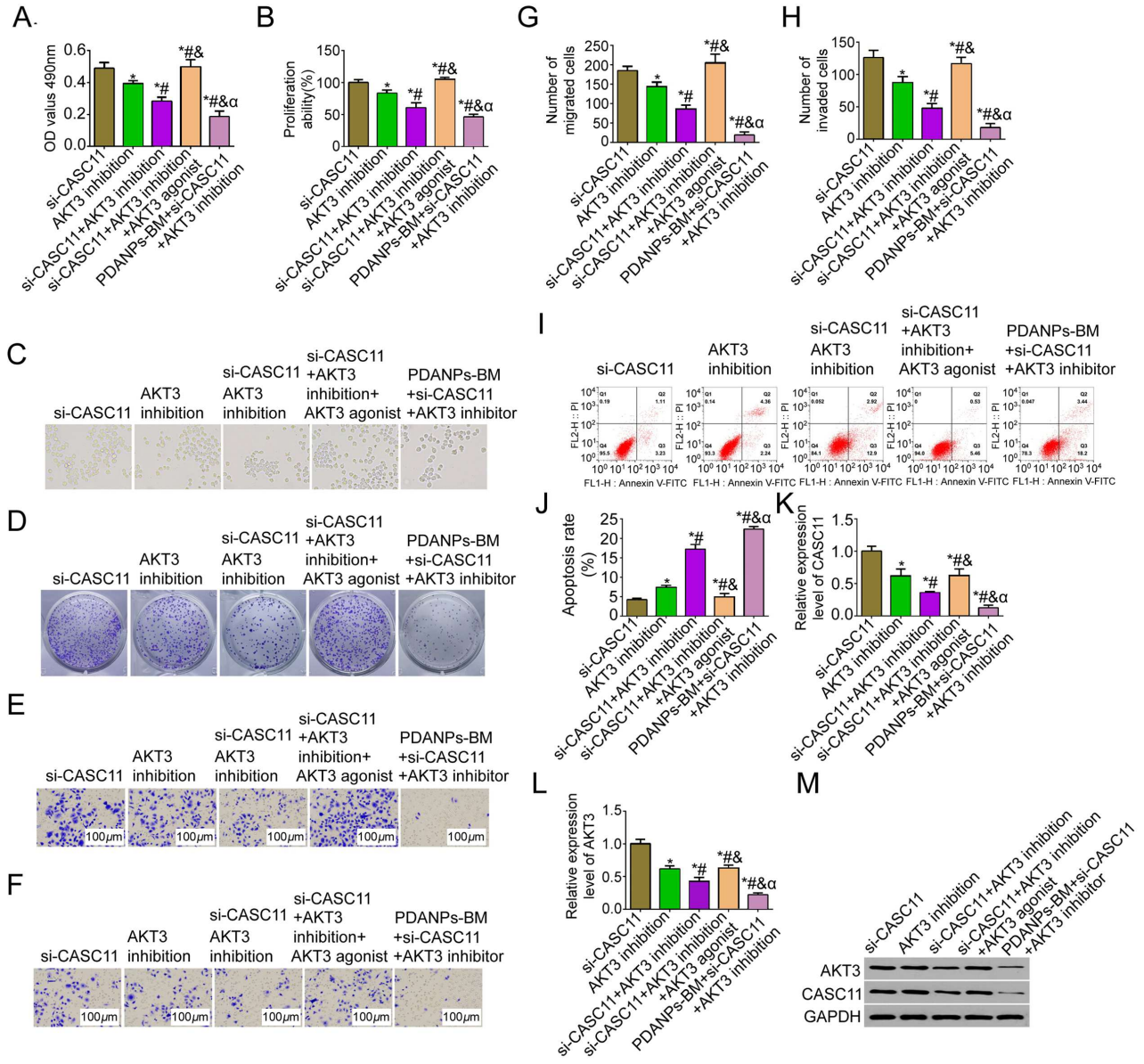

Fig. 5: PDANPs-BN slows down the malignant biological behavior of glioma through the CASC11/AKT3 axis. (A) MTT method to detect cell growth rate; (B) CCK-8 to detect cell proliferation ability; (C) MTT method to detect cell morphology; (D) Plate colony formation assay to detect cell formation ability; (E and F) Trans well detects cell migration ability; (G and H): Trans well detects cell invasion ability; (I and J) Flow cytometry detects cell apoptosis; (K and L) qRT-PCR method detects CASC11 and AKT3 relative gene expression level; (M) Western blot detects the protein expression of CASC11 and AKT3; compared with si-CASC11 group, *P<0.05; compared with AKT3 inhibitor group #P<0.05; compared with si-CASC11+AKT3 inhibition compared with the agent group and P<0.05; compared with the si-CASC11+AKT3 inhibitor+AKT3 activator group, α P<0.05; n=9.

DISCUSSION

In this study, a PDANPs-BN delivery system was successfully constructed and characterized and its superior efficacy over free BN in suppressing the proliferation, migration, invasion and survival of glioblastoma U251 cells *in-vitro* was demonstrated. Mechanistically, the gain- and loss-of-function experiments performed in this study strongly suggested that this enhanced anti-tumor activity was mediated, at least in part, through the downregulation of the oncogenic lncRNA CASC11 and consequent inhibition of its downstream effector, the brain-enriched kinase AKT3. This work not only provides novel evidence for the anti-glioma potential of BN but also positions the CASC11/AKT3 axis as a plausible and druggable signaling node in glioma, warranting further investigation.

The PDANPs-BN nanocomposites prepared in this study exhibited favorable physicochemical properties, including suitable nanoparticle size, negative surface potential, low polydispersity index and a high encapsulation efficiency of 85.4%. These characteristics aligned with the standards of an ideal nanodrug carrier, facilitating potential tumor targeting via the enhanced permeability and retention (EPR) effect while reducing non-specific clearance (Ma *et al*., 2023). FTIR spectroscopy confirmed the successful drug loading. More importantly, the study results consistently showed that PDANPs-BN outperformed free BN, an enhancement attributable not merely to drug delivery but also to the multifunctional advantages of the polydopamine-based carrier.

First, the PDA coating effectively protects BN from photolysis, hydrolysis, or enzymatic degradation in physiological environments, thereby preserving its bioactivity (Bezze *et al*., 2024). Second, the inherent adhesiveness and ease of functionalization of PDA may promote the interaction between nanoparticles and cell membranes, significantly enhancing cellular internalization of BN via pathways such as clathrin-mediated endocytosis or macropinocytosis (Shi *et al*., 2023). This resulted in higher intracellular drug accumulation and prolonged action, providing a stronger pharmacological foundation for targeting the CASC11/AKT3 axis. Moreover, the poor aqueous solubility and membrane permeability of free BN likely limit its cellular uptake, whereas nanoencapsulation fundamentally overcomes these physicochemical barriers.

Mechanistic investigations provided compelling, albeit correlative, evidence implicating the CASC11/AKT3 axis. A functional link was established by observing that siRNA-mediated knockdown of CASC11 or pharmacological inhibition of AKT3 synergized with PDANPs-BN, whereas overexpression of CASC11 or activation of AKT3 partially rescued the malignant phenotype. This finding aligns with the established oncogenic role of CASC11 in other cancers, where it often acts as a molecular scaffold or competitive endogenous RNA (ceRNA) to activate PI3K/AKT signaling (Wang *et al*., 2020; Capik *et al*., 2021). This association was validated in glioma, where CASC11 appeared to positively regulate AKT3, a brain-enriched kinase crucial for glioma proliferation, survival and therapy resistance (Shadbad and Baradaran, 2024).

Based on the data obtained in this study and prior knowledge, a plausible mechanistic model was proposed: PDANPs-BN, through efficient intracellular delivery of BN, may interfere with CASC11 transcription or stability, possibly by modulating epigenetic regulators (e.g., histone modifications or DNA methylation) or by interacting with transcription factors that govern CASC11 expression. Reduced CASC11 levels could weaken its scaffolding support for PDK1 or other adaptor proteins, leading to decreased phosphorylation and activation of AKT3. This, in turn, would downregulate downstream pro-survival effectors such as mTOR and NF-κB while enhancing pro-apoptotic signals, collectively curbing tumor growth and dissemination. However, whether BN directly binds CASC11 RNA or modulates its upstream regulators remains speculative and warrants further investigation via techniques such as RNA immunoprecipitation (RIP), chromatin immunoprecipitation (ChIP) or RNA-protein pull-down assays.

Beyond mechanistic novelty, the present study integrates a natural compound-based nanotherapy with lncRNA targeting, thereby presenting a combinatorial strategy. While previous research on PDA in glioma focused on drug delivery or photothermal therapy (Wu *et al*., 2022) and studies on BN highlighted pathways such as PPARγ/PTEN/Akt (Zhang *et al*., 2023), the present work is the first to converge on the CASC11/AKT3 axis in glioma. This axis-focused approach, in contrast to single-gene targeting, may offer a broader and more resilient intervention strategy against the adaptive signaling networks in glioma.

Despite the encouraging *in-vitro* results, the path to clinical translation is fraught with multifaceted challenges that this study has not addressed and must be rigorously evaluated: (1) The conclusions are derived from a single cell line (U251), which cannot capture the profound intra- and inter-tumoral heterogeneity of human gliomas. The immunosuppressive tumor microenvironment (TME)—including tumor-associated macrophages, microglia and regulatory T cells—may profoundly alter the efficacy of PDANPs-BN. Notably, the PI3K/AKT pathway is a known regulator of immune cell function. A critical yet unexplored question is whether PDANPs-BN-mediated AKT3 inhibition can reprogram the glioma TME; (2) Although the blood-brain barrier (BBB) is often disrupted in high-grade gliomas, its intact portions and the invasive tumor front remain significant barriers. The passive targeting via the enhanced permeability and retention (EPR) effect, which the current nanosystem relies on, is highly variable and often overestimated in preclinical models. Active targeting strategies are likely necessary to achieve sufficient therapeutic concentrations in the brain; (3) The long-term fate of PDA nanoparticles in the brain is not fully understood. Their degradation products, potential to induce neuroinflammation or gliosis and clearance mechanisms require detailed investigation. Preclinical pharmacokinetic/pharmacodynamic (PK/PD) studies must define the maximum tolerated dose, therapeutic window and dosing schedule; (4) Translating nanomedicines from the laboratory to the clinic requires overcoming practical obstacles. Reproducible, Good Manufacturing Practice (GMP)-compliant scale-up production of PDANPs-BN, ensuring batch-to-batch consistency in size, drug loading and sterility, is non-trivial.

Regulatory agencies will require extensive data on chemistry, manufacturing and controls (CMC), as well as safety, beyond that required for standard small-molecule drugs.

To systematically address these gaps and advance this therapeutic concept, a staged future research plan was proposed a staged future research plan; (1) *Validation in complex models*: A panel should be used of patient-derived glioma stem cell lines and 3D organoid cultures to evaluate efficacy across different molecular subtypes; (2) *In-depth mechanistic exploration*: RIP-seq should be utilized and ChIP-seq to identify the direct molecular interactors of CASC11 and the transcriptional regulators affected by BN; (3) *In-vivo proof-of-concept*: An orthotopic model should be established mouse glioma model to evaluate BBB penetration, biodistribution, anti-tumor efficacy and systemic toxicity of both passively and actively targeted PDANPs-BN variants; (4) *Immunomodulation studies*: Changes should be analyzed in the tumor immune microenvironment following treatment using flow cytometry and cytokine arrays; (5) *Preclinical development*: Investigational studies should be conducted New Drug (IND)-enabling studies, including Good Laboratory Practice (GLP) toxicology, PK/PD and formulation stability assessments.

CONCLUSION

In summary, PDANPs-BN demonstrate potent anti-glioma activity *in-vitro* by efficiently delivering BN and targeting inhibition of the CASC11/AKT3 signaling axis. This study not only unveils a novel mechanism underlying the action of BN but also demonstrates the potential of nanotechnology to enhance the efficacy of natural medicinal agents. While numerous scientific and translational challenges remain to be overcome on the path from laboratory research to clinical application, this work provides a valuable theoretical foundation and experimental starting point for the development of novel targeted nanotherapies for glioma.

Acknowledgments
Grateful acknowledgment is made to the Affiliated Hospital of Jiangnan University for providing the necessary equipment for this study.

Author's contributions
Leyuan Zhou: Conceptualization, methodology, investigation and formal analysis; Kaihua Yang: Writing - original draft, writing - review and editing. All authors have read and agreed to the published version of the manuscript.

Funding
There was no funding.

Data availability statement
The datasets generated during and/or analysed during the current study are available from the corresponding author on reasonable request.

Ethics approval
This study utilized only cell lines and all experimental procedures were conducted in accordance with the regulations of the Ethics Committee of Affiliated Hospital of Jiangnan University (Approval No.: LS2025522).

Conflicts of interest
The authors declare no conflict of interest.

REFERENCES

Bashir K, Khan MFA, Alhodaib A, Ahmed N, Naz I, Mirza B, Tipu MK and Fatima H (2022). Design and evaluation of pH-sensitive nanoformulation of bergenin isolated from bergenia ciliata. *Polymers (Basel)*., **14**(9): 1639.

Bezze A, Mattioda C, Ciardelli G and Mattu C (2024). Harnessing cells to improve transport of nanomedicines. *Eur J Pharm Biopharm*., **203**: 114446.

Brix N, Samaga D, Belka C, Zitzelsberger H and Lauber K (2021). Analysis of clonogenic growth *in-vitro*. *Nat Protoc*., **16**(11): 4963–4991.

Cao L, Weng K, Li L, Lin G, Zhao Y, Gao Y, Huang X, Chen Q, Wang J, Zheng C, Huang C, Xie J and Li P (2024). BATF2 inhibits the stem cell-like properties and chemoresistance of gastric cancer cells through PTEN/AKT/β-catenin pathway. *Theranostics*., **14**(18): 7007–7022.

Capik O, Sanli F, Kurt A, Ceylan O, Suer I, Kaya M, Ittmann M and Karatas OF (2021). CASC11 promotes aggressiveness of prostate cancer cells through miR-145/IGF1R axis. *Prostate Cancer Prostatic Dis*., **24**(3): 891–902.

He J, Han J, Lin K, Wang J, Li G, Li X and Gao Y (2023). PTEN/AKT and Wnt/β-catenin signaling pathways regulate the proliferation of Lgr5+ cells in liver cancer. *Biochem Biophys Res Commun*.,**683**: 149117.

Han C, Chen C, Lu N, Xue L, Xing D, Wu W, Li W and Lu X (2024). Platelet-rich plasma inhibits breast cancer proliferation. *Clin Med Insights Oncol*., **18**: 11795549241298978.

Hu Z, Ghosh A and Koncz C (2022). Plant gene modification by BAC recombineering. *Methods Mol Biol*., **2479**: 71–84.

Hu K, Zhang D, Ma W, Gu Y, Zhao J and Mu X (2024). Polydopamine-based nanoparticles for synergistic chemotherapy of prostate cancer. *Int J Nanomedicine*., **19**: 6717–6730.

Li X, Xie L, Zhou L, Gan Y, Han S, Zhou Y, Qing X and Li W (2023). Bergenin inhibits tumor growth and

overcomes radioresistance by targeting aerobic glycolysis. *Am J Chin Med*., **51**(7): 1905–1925.

Lin H, Wang P, Zhang W, Yan H, Yu H, Yan L, Chen H, Xie M and Shan L (2022). Novel combined preparation and investigation of bergenin-loaded albumin nanoparticles for the treatment of acute lung injury: *In-vitro* and *in-vivo* evaluations. *Inflammation*., **45**(1): 428–444.

Li J, Feng X, Jiang H, Mo X, Liu C, Liu X, Feng T and Zhou Y (2025). Near-infrared and pH-responsive carbon dots/bergenin for biological imaging and chemo-photothermal synergistic tumor therapy. *J Colloid Interface Sci*., **694**: 137679.

Ma B, Ma Y, Deng B, Xiao P, Huang P, Wang D and Liu L (2023). Tumor microenvironment-responsive spherical nucleic acid nanoparticles for enhanced chemo-immunotherapy. *J Nanobiotechnology*., **21**(1): 171.

Mahata R, Manna S, Modak M and Choudhury SM (2025). A review on the advancement of polydopamine (PDA)-based nanomaterials for cancer treatment. *Med Oncol*., **42**(5):165.

Moradi MT, Altememy D, Asadi-Samani M, Khosravian P, Soltani M, Hashemi L and Samiei-Sefat A (2024). The effect of celastrol in combination with 5-fluorouracil on proliferation and apoptosis of gastric cancer cell lines. *Oncol Res*., **32**(7): 1231–1237.

Petrillo S, Carra G, Bottino P, Zanotto E, De Santis MC, Margaria JP, Giorgio A, Mandili G, Martini M, Cavallo R, Barberio D and Altruda F (2020). A novel multiplex qRT-PCR assay to detect SARS-CoV-2 infection: High sensitivity and increased testing capacity. *Microorganisms*., **8**(7): 1064.

Read RD, Tapp ZM, Rajappa P and Hambardzumyan D (2024). Glioblastoma microenvironment-from biology to therapy. *Genes Dev*., **38**(9-10): 360–379.

Shi Q, Wu Y, Xu Y, Bao M, Chen X, Huang K, Yang Q and Yang Y (2023). Virus mimetic framework DNA as a Non-LNP gene carrier for modulated cell endocytosis and apoptosis. *ACS Nano*., **17**(3): 2460–2471.

Shadbad MA and Baradaran B (2024). hsa-miR-181a-5p inhibits glioblastoma development via the MAPK pathway: *In-silico* and *in-vitro* study. *Oncol Res*., **32**(12): 1949–1958.

Smith PK, Krohn RI, Hermanson GT, Mallia AK, Gartner FH, Provenzano MD, Fujimoto EK, Goeke NM, Olson BJ and Klenk DC (1985). Measurement of protein using bicinchoninic acid. *Anal Biochem*., **150**(1): 76–85.

Towbin H, Staehelin T and Gordon J (1979). Electrophoretic transfer of proteins from polyacrylamide gels to nitrocellulose sheets: Procedure and some applications. *Proc Natl Acad Sci USA*., **76**(9): 4350–4354.

Wang B, Xu W, Hu C, Liu K, Chen J, Guo C and Yuan C (2020). Critical roles of the lncRNA CASC11 in tumor progression and cancer metastasis: The biomarker and therapeutic target potential. *Genes Dis*., **9**(2): 325–333.

Wu H, Wei M, Xu Y, Li Y, Zhai X, Su P, Ma Q and Zhang H (2022). PDA-based drug delivery nanosystems: A potential approach for glioma treatment. *Int J Nanomedicine*., **17**: 3751–3775.

Yan H, Sun Y, Wu Q, Wu Z, Hu M, Sun Y, Liu Y, Ma Z, Liu S, Xiao W, Liu F and Ning Z (2020). PELP1 suppression inhibits gastric cancer through downregulation of c-Src-PI3K-ERK pathway. *Front Oncol*., **9**: 1423.

Zhuo S, Yang L, Chen Z, Chen S, Yang S, Chen T, Wu WS, Wang K and Yang K (2025). Druggable target ATAD2 enhances the malignant progression and cooperates with E2F1 to up-regulate PDK1 expression in glioma. *Genes Dis*., **13**(1): 101810.

Zhao K, Gao J, Shi J, Shi C, Pang C, Li J, Guo W and Zhang S (2022). FXR1 promotes proliferation, invasion and migration of hepatocellular carcinoma *in-vitro* and *In-vivo*. *Oncol Lett*., **25**(1): 22.

Zheng Y, Wang Y, Li J, Zheng S, Zhang L, Li Q, Ling F, Nie Q, Feng Q, Wang J and Jin C (2025). PGAM5 modulates macrophage polarization, aggravating inflammation in COPD via the NF-κB pathway. *Int J Chron Obstruct Pulmon Dis*., **20**: 551–564.

Zhang P, Sun Y, Shi L, Sun D, Wang L, Feng D and Ding C (2023). Effect of isorhamnetin on carbonic anhydrase IX expression and tumorigenesis of bladder cancer by activating PPARγ/PTEN/AKT pathway. *Tissue Cell*., **82**: 102048.

Zheng L, Guan Z and Xue M (2021). A crucial role for the long non-coding RNA CASC11 in the pathogenesis of human cancers. *Am J Transl Res*., **13**(9): 10922–10932.